Biophysical Journal Volume 100 May 2011 2530–2538

Structural and Mechanical Analysis of Tectorial Membrane *Tecta* Mutants

Rachel Gueta,[†] Jonathan Levitt,[‡] Anping Xia,[§] Ori Katz,[‡] John S. Oghalai,[§] and Itay Rousso[†*]
[†]Department of Structural Biology and [‡]Department of Physics of Complex Systems, Weizmann Institute of Science, Rehovot, Israel; and [§]Department of Otolaryngology—Head and Neck Surgery, Stanford University, Stanford, California

ABSTRACT The tectorial membrane (TM) is an extracellular matrix of the cochlea whose prominent role in hearing has been demonstrated through mutation studies. The C1509G mutation of the *Tecta* gene, which encodes for the α-tectorin protein, leads to hearing loss. The heterozygote TM only attaches to the first row of outer hair cells (OHCs), and the homozygote TM does not attach to any OHCs. Here we measured the morphology and mechanical properties of wild-type, heterozygous, and homozygous *Tecta* TMs. Morphological analyses conducted with second- and third-harmonic imaging, scanning electron microscopy, and immunolabeling revealed marked changes in the collagen architecture and stereocilin-labeling patterns of the mutant TMs. The mechanical properties of the mutant TM were measured by force spectroscopy. Whereas the axial Young's modulus of the low-frequency (apical) region of *Tecta* mutant TM samples was similar to that of wild-type TMs, it significantly decreased in the basal region to a value approaching that found at the apex. Modeling simulations suggest that a reduced TM Young's modulus is likely to reduce OHC stereociliary deflection. These findings argue that the heterozygote C1509G mutation results in a lack of attachment of the TM to the OHCs, which in turn reduces both the overall number of OHCs that are involved in mechanotransduction and the degree of mechanotransduction exhibited by the OHCs that remain attached to the TM.

INTRODUCTION

Collagen accounts for ~50% of the constituent proteins of the tectorial membrane (TM), a highly hydrated extracellular matrix located in the mammalian cochlea. The radial fibrils of the TM consist mostly of collagen type II and are embedded in a striated sheet matrix made of two types of proteins that are exclusively expressed in the TM: α-tectorin and β-tectorin (1–3).

As with other collagen-based matrices, the material properties of the TM are governed by the morphology and organization of the collagen fibers. In a previous study (4), an indentation analysis using atomic force microscopy (AFM) revealed a clear correlation between the stiffness of the TM and its longitudinal and radial positions. Specifically, a gradual increase was detected in the stiffness of the TM in the hair-cells (HC) zone from its apical to basilar ends along the length of the cochlea. Scanning electron microscope (SEM) analysis of the TM revealed clear changes to the fiber arrangement in the radial and longitudinal directions, which correlated with the results obtained from the indentation assays. Most notably, it was found that, proceeding toward the basilar region, the collagen fibers gradually merged until they formed a tightly packed structure, correlating with the 10-fold increase in stiffness measured in this area. Additionally, the anisotropic properties of the TM were shown to be highly correlated with collagen fibril organization (5–8). Larger elastic modulus values were found at the basal end of the cochlea than at the apical end, which was attributed to the increased collagen fiber thickness and denser packing arrangement observed at the basal end (7).

A further understanding of the interrelations between the arrangement of the collagen fibers and TM mechanical properties can be obtained from measurements of mutated TM samples. TM segments isolated from mice with a targeted deletion of Col11a2, which encodes for collagen XI, were shown to have significantly lower fiber density than wild-type (WT) TM (9). A comparison between the mechanical shear impedance measurements of Col11a2 and WT TMs suggested a linkage between the organization of the collagen fibers into radial fibrils and the mechanical anisotropy of the TM (10).

By virtue of its nature, the TM is expected to play a mechanical role in cochlear function. Understanding the role of the TM thus requires a detailed knowledge of its mechanical properties. Recent results from several studies (4,8,11,12) have strengthened the link between the mechanical properties and biological role of the TM. In one such study, we found a large variation in the elastic modulus along the longitudinal direction of the TM within the zone that is located above the auditory sensory cells (4). This finding, which was later confirmed and extended by two other groups (11,12), suggests that the TM is mechanically coupled with other organs in the cochlea, such as the outer hair cells (OHCs), and thus may enhance cochlear sensitivity and tuning. In another study, the anisotropic material properties of the TM were determined under a newly established framework that combines simulations and experiments (8). This study provided evidence that the deflection of stereocilium bundles is enabled by the anisotropic properties of the TM.

In the study presented here, to gain more insights into the interplay among the structure, mechanical properties, and biological role of the TM, we analyzed samples isolated from knock-in mice containing the C1509G point mutation

Submitted December 26, 2010, and accepted for publication April 4, 2011.
*Correspondence: itay.rousso@weizmann.ac.il
Editor: James R. Sellers.

0006-3495/11/05/2530/9 $2.00
doi: 10.1016/j.bpj.2011.04.024

in the *Tecta* gene (13). The *Tecta* gene encodes the α-tectorin protein of the TM. In humans, this mutation causes partial hearing loss that is worse at higher frequencies (14). Auditory brain response (ABR) and distortion product otoacoustic emission (DPOAE) analyses in mice showed significant threshold increases that were most prominent at the middle and high frequencies (25–40 and 30–50 dB for heterozygous ($Tecta^{C1509G/+}$) and homozygous ($Tecta^{C1509G/1509G}$) mice, respectively (13)). Morphological analysis of cochlear sections revealed anatomical differences among two genotypes and the WT in the basilar section of the TM (13). The basilar section of the TM of heterozygous mice was shorter in the radial direction and covered only the first row of OHC stereocilia. In homozygous mice, the basilar section of the TM appeared to be loosely connected to the spiral limbus and elevated above the organ of Corti, resulting in a complete detachment from the OHC stereocilia. Transmission electron microscopy (TEM) images revealed marked changes in the organization of the fibers along the edge of the TM in the basilar OHC zone. In contrast to the WT TM, whose fibers are tightly packed in this region, partial disruption is observed in the heterozygous samples, whereas homozygous TM samples show severe disruption (13). In this study we analyzed the structure and mechanical properties of both heterozygous and homozygous *Tecta* TM samples. Our results offer a possible mechanical interpretation for the physiological effect of the heterozygous *Tecta* mutation.

MATERIALS AND METHODS

Sample preparation

We isolated TM samples from a total of 29 heterozygous and homozygous adult mice (~2 months old) using previously reported techniques (5). The TM pieces were classified along the longitudinal axis of the cochlea based on their dimensions. Wide and thick samples were considered to be associated with the apical region of the cochlea, whereas narrower and thinner samples were considered to be taken from the basilar region. Pieces that could not be assigned to either end were considered to be extracted from the mid-turn region. The measurements were focused on the OHC radial zone, which represents the area of the TM that covers the stereocilia bundles of the HCs. Isolated TM samples were attached to Cell-Tak-coated glass slides.

Electron microscopy

After isolated TM segments adhered to the Cell-Tak-coated glass slides, the samples were incubated in a solution of 2% glutaraldehyde in 0.1 M sodium cacodylate buffer (pH 7.4) for ~24 h. After fixation was completed, the samples were washed three times with 0.1 M sodium cacodylate buffer and immersed in 1% OsO_4 solution for 1 h. The samples were then immersed in 1% tannic acid for 5 min, followed by a 30-min incubation in 1% uranyl acetate solution. Between each treatment, the samples were rinsed three times with distilled water. After rinsing, the samples were dehydrated by a set of solutions characterized by increasing ethanol concentration, followed by critical point drying with liquid CO_2. The TM pieces were imaged with the use of an environmental scanning electron microscope (Phillips XL-30, Eindhoven, The Netherlands).

Second- and third-harmonic imaging microscopy

Second- and third-harmonic generation microscopy images were obtained with the use of an inverted microscope (Axiovert 135; Carl Zeiss, Jena, Germany) modified for laser scanning. The laser source was a Tsunami Ti: Sapphire oscillator that delivered linearly polarized 100 fs pulses centered around 808 nm at a repetition rate of 80 MHz. The laser was focused onto the sample by means of a super apochromatic 60×, 1.20 numerical aperture, water-immersion objective (UPLSAPO 60XW; Olympus, Tokyo, Japan). A pump power of ~45 mW was measured before the objective. The focal point was raster scanned at 500 Hz in the *xy* plane with galvanometer mirrors (Cambridge Technology, Lexington, MA), and in the *z* axis with a piezo objective mount (NV 40/1 CLE; Piezosystem, Jena, Germany). Emitted light was collimated in the forward direction with an f = 16 mm fused silica condenser (LINOS Photonics, Munich, Germany). A dichroic mirror (FF310-Di01; Semrock, Rochester, NY) was used to separate the second- and third-harmonic photons. The second-harmonic photons passed through shortpass and bandpass filters (720/SP, 406/15; Semrock, Rochester, NY) and were measured by a R4220 photomultiplier (Hamamatsu, Hamamatsu City, Japan). Third-harmonic photons passed through a 266 ± 5 nm bandpass filter and were measured by an R7154 photomultiplier (Hamamatsu, Japan). The current generated by each photomultiplier was amplified with a low-noise current amplifier (SR-750; Stanford Research Systems, Sunnyvale, CA) and digitized with the use of a PCI-6024E controlled by LabView (National Instruments, Austin, TX). Imaris imaging software (Bitplane, Zurich, Switzerland) was used to process the images.

Immunolabeling

Tecta mice at postnatal day 15 were euthanized. Each cochlea was isolated from the temporal bone in cold phosphate-buffered solution (PBS) and fixed in 4% paraformaldehyde for 1 h at room temperature. After washing with PBS, the membranous labyrinth was dissected out and immersed in blocking solution (5% goat serum, 0.1% Triton X-100, 1% bovine serum albumin (BSA), and 0.02% sodium azide (NaN_3) in PBS) for 1 h at room temperature. It was then incubated with rabbit anti-stereocilin primary antibody (a gift from Christine Petit (15)) at a 1:150 dilution in blocking solution overnight at 4°C. The next day, the tissue was rinsed with PBST (0.1% Triton X-100 in PBS) three times, and then immersed with Alexa Fluor 546 goat anti-rabbit secondary antibody (Invitrogen, Carlsbad, CA) in a solution (0.1% Triton X-100, 1% BSA, and 0.02% NaN_3 solution in PBS) at room temperature for 1 h. After washing with PBST again, the bony modiolus was removed, the upper part of spiral ligament was cut off, and the TM was gently removed with a fine forceps. The membranous labyrinth and the TM were mounted in anti-fade fluorescence mounting medium (DAKO, Carpinteria, CA) and coverslipped. Images were captured by epifluorescent (TM images) or confocal microscopy (stereociliary bundle images; Axioplan 2, Zeiss, Germany) and analyzed with the use of Photoshop CS4 (Adobe Systems, San Jose, CA) or Volocity software (v5.3.0; Improvision, Waltham, MA).

AFM measurements

For all of the AFM experiments, we used a Bioscope with a Nanoscope IV controller (Veeco, Santa Barbara, CA) mounted on an inverted optical microscope (IX70; Olympus). AFM measurements were carried out with the use of borosilicate spherical probes (diameter = ~2 μm; Bioforce, Ames, IA) attached to silicon triangular cantilevers with a nominal spring constant of 0.08 N/m. We determined the spring constant of the cantilever experimentally by measuring the thermal fluctuations (16). The normal stiffness of the TM was determined based on indentation-type experiments, as previously described (4). Briefly, for each indentation measurement, we obtained 100 force-distance curves at a scan rate of 2 Hz. The maximal applied loading force in each measurement was ~30 nN. We calculated the Young's modulus by fitting a modified Hertz model to the upper 75%

of the force-distance curves. With this method, it is possible that repeated applications of force might irreversibly damage the sample, or, alternatively, that the loading rate might affect the measured stiffness. Therefore, for each measurement consisting of ~100 force-distance curves, we plotted the measured point stiffness derived from each curve as a function of the measurement number, and as a histogram (see the Supporting Material). During each experiment, the measured stiffness values derived from the individual force-distance curves were found to distribute normally around a mean, which suggests that the virus did not undergo irreversible deformation during measurement.

Lateral-force measurements

Before each lateral-force measurement, we obtained a force-distance curve to determine the indentation depth of the sample at any given loading force. We then oscillated the AFM probe perpendicular to the long axis of the cantilever by driving the piezo scanner using an external function generator (Agilent, Santa Clara, CA). The driving triangular signal and the cantilever torsion were acquired by a data acquisition card and on a computer running LabView. The torsion signal was then grouped to lateral load and unload according to the driving signal slope. Next, the signals within each group were averaged. The acquisition time for each measurement was ~60 s, which corresponds to the averaging of ~60 lateral-force curves. Finally, to convert the torsion signal from volts to unit of force (nN), we used the calibration method described by Ruan and Bhushan (17). A detailed description of the methodology used for measuring the lateral stiffness was described previously (8).

Finite-element simulation

Modeling lateral-force measurements

To estimate the lateral mechanical properties of the heterozygous TM, we simulated the lateral-force experiments using the finite-element method. The TM was modeled as a three-dimensional (3D) plate resting on a flat rigid surface and loaded by an absolutely rigid 2 μm spherical indenter. Sliding frictionless contact was assumed between the flat substrate and the TM model, and between the indenter and the TM. The presence of contact and large displacements creates a nonlinear problem. Therefore, the numerical model assumed nonlinear geometric kinematics (allowing for large displacements) but linear elastic material behavior as the available approximation. This problem was solved by MSC.MARC software. Loading was simulated by prescribing the downward movement of the rigid indenter, calculated in 25 consecutive increments. Next, during maximal indentation, the indenter was laterally displaced in 100 consecutive increments. The magnitudes of the simulated lateral displacement and indentation were similar to their experimental counterparts.

Modeling TM-stereocilia mechanical interactions

To simulate the interactions between the heterozygous TM and a stereocilium, the TM was simulated as a 3D plate as in the previous simulation. The stereocilium was modeled as a nondeformable rod capped by a sphere, and was 150 nm in diameter. It was oriented at a 20° angle with respect to the TM surface, and its tip was embedded 100 nm inside the TM. To simulate stereocilia motion, the stereocilium was pushed against the TM from its base in the direction of the initial position of its longitudinal axis. The amplitude of the motion was 300 nm. During this movement, the rod rotational movement was unconstrained. The experimentally derived moduli were incorporated into the TM model. This problem was solved by MSC.MARC software and the results were rendered by Hyperview (Altair, Troy, MI).

RESULTS AND DISCUSSION

Structural analysis of WT, heterozygous, and homozygous TM samples

A standard light-microscopy analysis reveals clear differences between the morphology of the three TM genotypes. The major morphological difference between heterozygous and homozygous TMs is expressed mainly in the HC and limbal zones of the basilar TM section. In the basilar part of WT TM samples, the margin between the HC, main body (MB), and limbal zones is clearly visible. Even by light microscopy, the parallel arrangement of the fibers can be detected, and the appearance of the marginal band is observed in the HC zone (Fig. 1 *A*). Samples isolated from the basilar region of the cochlea of heterozygous TMs appear narrower than those isolated from WT TMs, mainly due to the disruption of the fibers in the HC and limbal zones (Fig. 1 *B*). The limbal zone is thinner and narrower, and the HC zone is partially unraveled. In addition, no clear margin between the MB and HC regions is observed, due to the absence of Hensen's stripe. The limbal zone of the basilar section of the homozygous TM appears

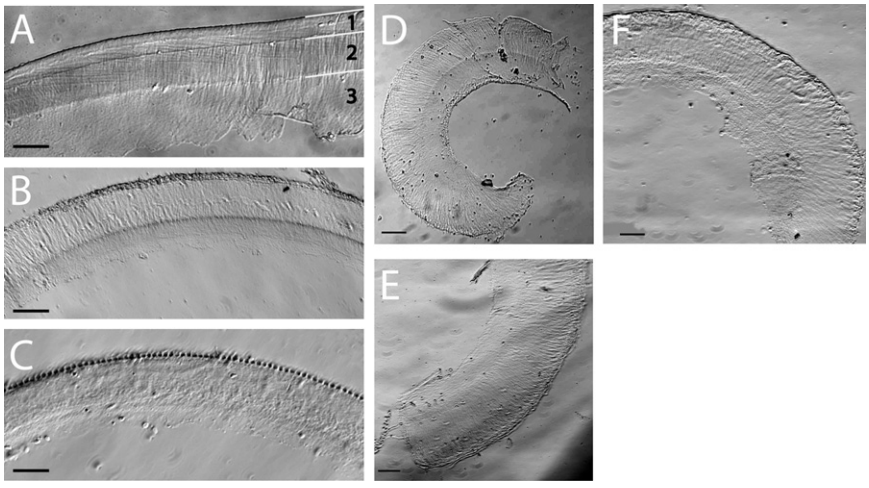

FIGURE 1 Morphology of the three *Tecta* genotypes. (*A–C*) Phase-contrast transmitted light-microscopy images of WT (*A*), heterozygous (*B*), and homozygous (*C*) TM samples isolated from the basilar region of the cochlea. The partial structural disruption of the heterozygous TM and the heavily serrated edge of the HC zone of the homozygous TM are clearly visible. (*D–F*) Images of (*D*) WT, (*E*) heterozygous, and (*F*) homozygous TM samples isolated from the apical region of the cochlea. The morphology of all three genotypes appears to be similar. Numbers in *A* relate to the three radial zones (i.e., the HC, MB, and limbal zones), which are labeled as 1, 2 and 3, respectively. Scale bars represent 50 μm.

to be damaged in its entirety and is much thinner and narrower than that of the WT. In the HC zone, a clear serrated edge is observed (Fig. 1 *C*). In the apical part of the cochlea, there are no visible differences between the three TM genotypes, and the parallel collagen arrangement along the radial direction in the limbal and HC zones appears wholly intact (Fig. 1, *D–F*).

Further investigation of the ultrastructure of the mutated TMs by SEM strengthened the optical microscope observations and revealed the organization of the fibers at the surface in the longitudinal and radial directions (Fig. 2, *A–D*). The apical section of the homozygous TM (Fig. 2 *B*) has a structure similar to that of WT TM, having the same fiber morphology and arrangement, i.e., parallel collagen fibers arranged along the radial direction of the TM (4). Proceeding toward the basilar end, the most dramatic changes are observed in the HC zone, which is partially serrated in the heterozygous TM (Fig. 2 *D*) and completely destroyed in the homozygous TM (Fig. 2 *C*). Additionally, in both mutated TMs, there is no remnant of the dense packing and parallel arrangement of fibers in the HC zone, as observed in the WT TM (4). Overall, the HC and MB zones of the basilar section of the mutated TMs appear to be entirely disordered. A possible explanation for the above observations is that the lack of α-tectorin as the matrix in between the fibers causes the collagen fibers to be more susceptible to fixation and dehydration treatments.

3D organization of the collagen fibers of native untreated TM samples from mutant mice

Fresh untreated samples from WT, heterozygous, and homozygous TMs were imaged by two-photon microscopy in an artificial endolymph (AE) buffer environment ~2 h after they were isolated from the cochlea. Fig. 3 shows second- and third-harmonic imaging microscopy (SHIM (*red*) and THIM (*green*), respectively) pictures of samples isolated from the apical and basilar regions of the three TM genotypes. SHIM is based on a nonlinear optical effect called second-harmonic generation. When light of high intensity (typically above several GW/cm^2) is focused inside a noncentrosymmetric material, photons with a frequency equal to twice the pumping laser frequency are generated coherently (18). We applied this method to analyze the 3D organization of the collagen fibers within WT TM samples (19). The THIM signal, on the other hand, which indicates changes in the interface between two materials that have a different refraction index (20), clearly emphasizes the contour of the TM samples in the 3D reconstruction images. The large panels of Fig. 3 show typical sections taken from the middle part of each TM sample, whereas the lower panels show a cross-sectional analysis of the reconstructed 3D images.

An analysis of the arrangement of fibers in the apical part of the TM reveals structural similarities between the three TM genotypes (Fig. 3). In sections that are close to the TM surface, the collagen fibers are arranged parallel to the surface plane. Throughout the interior depth of the TM samples, the fibers are tilted at an angle relative to the surface. This is indicated by the appearance of short fragments of fibers in the large upper panels, and is visualized directly in the cross-sectional analysis displayed in the lower panels. The cross-sectional images also show the transition from a tilted to a parallel orientation of the fibers in all three types of TM samples (Fig. 3, *lower panels*). However, the fiber density appears to be lower in the homozygous TM compared with the WT and heterozygous TM.

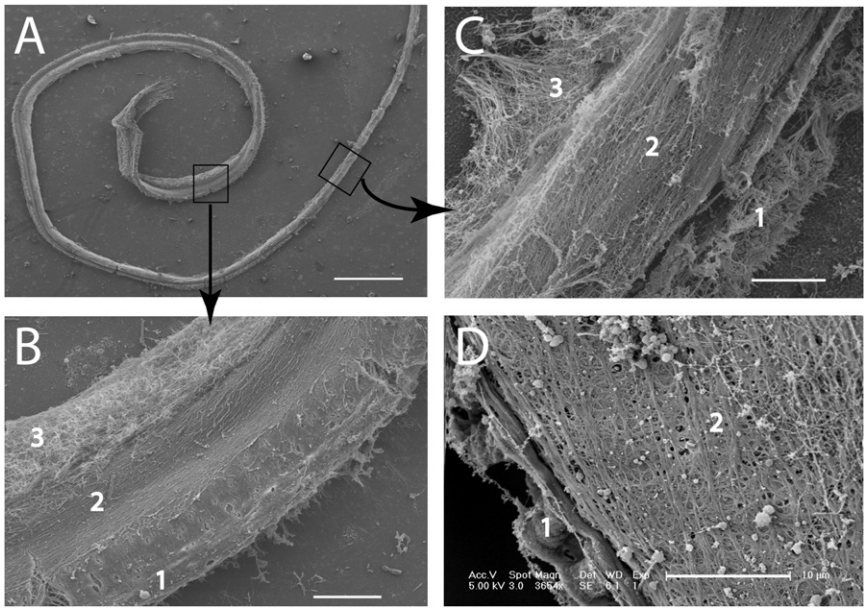

FIGURE 2 SEM analysis of the ultrastructure of the hetero- and homozygous *Tecta* TM. (*A*) A nearly complete segment of a homozygous *Tecta* TM sample. (*B*) A magnified image of a segment isolated from the apical region of the cochlea, showing an intact segment with a structure similar to that of WT TM. (*C* and *D*) Images of (*C*) homozygous and (*D*) heterozygous TM segments isolated from the basal end of the cochlea. The partially and completely serrated HC zone can be clearly seen in the hetero- and homozygote samples, respectively. Numbers on the images relate to the three radial zones (i.e., the HC, MB, and limbal zones), which are labeled as 1, 2 and 3, respectively. The scale bars for *A–D* are 200, 20, 10, and 10 μm, respectively.

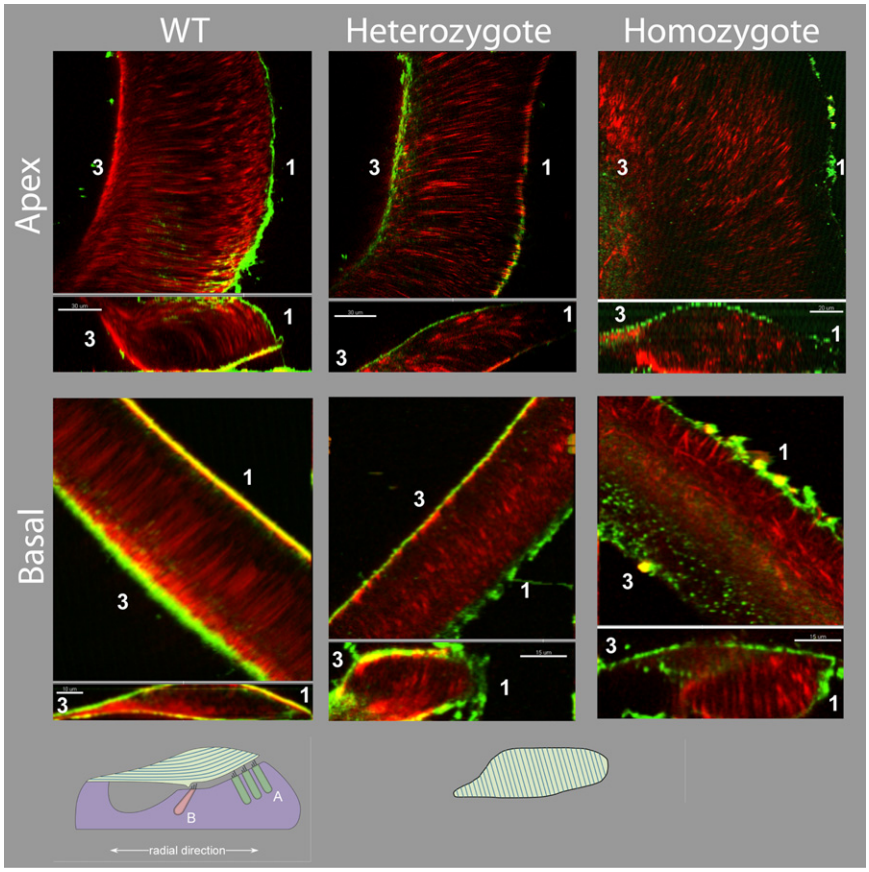

FIGURE 3 Second- and third-harmonic images (colored in *red* and *green*, respectively) of WT and hetero- and homozygous TM samples. The HC and limbal radial sides of the TM are labeled 1 and 3, respectively. The large panels show typical sections taken parallel to the surface of the TM representing its internal structure. The small panels show 3D cross-sectional images representing a plane perpendicular to the TM surface. Whereas the structure of the apical region appears to be hardly affected by the *Tecta* mutation, striking structural differences among the three genotypes are observed in the basilar region. The scale bars for WT and hetero- and homozygous apical TMs are 30, 30, and 20 μm, respectively. For basilar WT and hetero- and homozygous TMs, the scale bars are 10, 15, and 15 μm, respectively. The lower panel displays a schematic representation of the organ of Corti showing the location of the TM in relation to the (*A*) OHCs and (*B*) inner HCs in the cochlea. The most significant changes in the arrangements of the collagen fibers inside the TM, based on the results of the SHIM analysis, are shown. At the basal region of the cochlea, the fibers in WT TM are arranged in parallel orientation. In contrast, at the basal region of the cochlea, hetero- and homozygous TM samples are significantly thicker and the fiber orientation is tilted by nearly 90° compared with the WT.

In the basilar region, there are large differences in the fiber arrangements between TM samples isolated from WT, heterozygous, and homozygous mice (Fig. 3, *lower row*). In agreement with a previous observation (19), fibers in the WT TM are oriented strictly in parallel to each other and to the TM surface throughout the entire thickness of the TM (Fig. 3). In addition, an intensified signal representing the uniform matrix that covers the section of the TM that faces the OHCs (19) is observed along the edge of the HC zone throughout the thickness of the TM (Fig. 3, *upper panel*) and in the 3D reconstruction (Fig. 3, *lower panel*). On the basis of the 3D reconstruction, it can be seen that the convex shape at the HC zone of the basilar TM isolated from WT mice is highly preserved. The overall thickness of both mutated basilar TM samples is much larger than their WT counterpart, as observed previously (13). The organization of the fibers in the basilar heterozygous TM, however, resembles the fiber organization of the apical section. Fibers in the sample bulk are arranged at an angle with respect to the surface of the TM and in parallel with each other (Fig. 3). In the homozygous TM isolated from the basal part of the cochlea, the misalignment of the collagen fibers relative to each other and to the TM surface is clearly observed throughout the entire thickness of the TM (Fig. 3). In addition, instead of the intensified band in the HC zone of the WT TM, a partially or completely serrated edge is observed in the THIM signal from the same zone in hetero- and homozygous TM samples.

Stereocilin labeling

Stereocilin is a protein that is produced within HCs and localizes to the horizontal top connectors and the tips of the stereociliary bundles (21). In OHCs, it is thought to be related to the point of attachment between the stereocilia and the TM (22). When the TM is peeled off the HC epithelium, immunolabeling demonstrates the V-shaped pattern associated with the tallest row of the OHC stereociliary bundle (15).

Because *Tecta*$^{C1509/+}$ and *Tecta*$^{C1509G/C1509G}$ mice have disorganization of the collagen within the HC region, the area on the undersurface of the TM that interfaces with OHCs, we studied the impact of this mutation on stereocilin labeling in these transgenic mice (Fig. 4). We found that OHCs in all three genotypes demonstrated identical stereocilin immunolabeling, in that all three rows of OHCs had labeling within their stereocilia (Fig. 4 *A*). However, there were differences in their labeling patterns within the TM. The TM from WT mice demonstrated the expected V-shaped pattern of stereocilin for all three rows of OHCs.

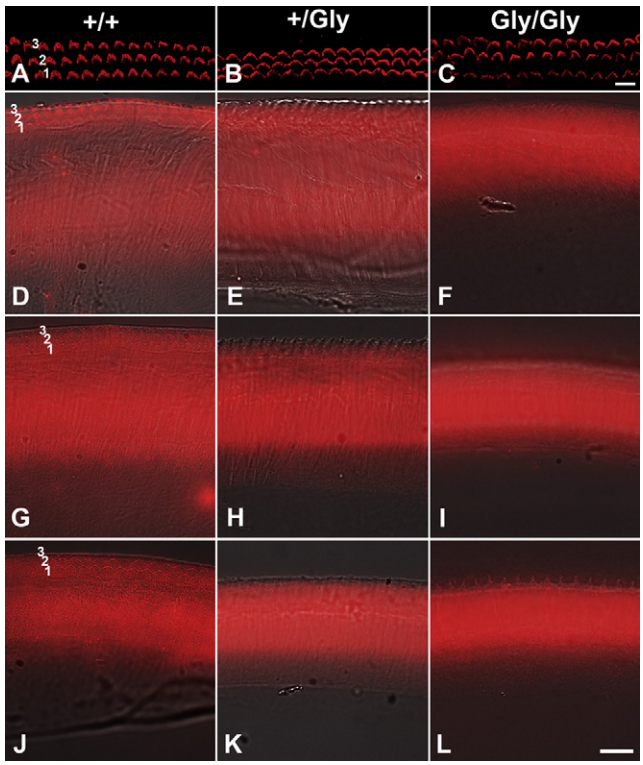

FIGURE 4 Stereocilin immunolabeling in the stereocilia and TM of P15 *Tecta* mice. (*A–C*) Middle turn: Stereocilin is expressed in the three rows of OHC stereocilia of all three genotypes (+/+, WT; +/Gly, heterozygote; Gly/Gly, homozygote). (*D*, *G*, and *J*) Stereocilin labeling in the TM defines the imprints of rows 1–3 of OHC stereocilia of all turns for WT mice but not in heterozygote (*E*, *H*, and *K*) or homozygote (*F*, *I* and *L*) mice. In addition, the TM is narrowed in the middle (*H* and *I*) and apical (*K* and *L*) turns in both the heterozygote and homozygote compared with the WT TM (*G* and *J*). *A–C*, bar = 10 μm; *D–L*, bar = 20 μm.

The immunolabeling strength was stronger in the base, but there was clear labeling in the middle and apical regions of the cochlea as well. However, neither the $Tecta^{C1509/+}$ nor the $Tecta^{C1509G/C1509G}$ mice demonstrated any stereocilin labeling in any of the three regions of the cochlea studied ($n = 6$ cochlea from each genotype). This indicates that 1), stereocilin produced by OHCs does not link to the TM; or 2), when the TM is peeled off the HC epithelium, the portion of the TM bound to stereocilin separates to stay with the OHC stereociliary bundle. In either case, these data further demonstrate the impact of the TM collagen disorganization associated with the $Tecta^{C1509G}$ mutation.

Mechanical properties of heterozygous and homozygous TM samples

To measure the normal stiffness of the TM, we positioned an AFM cantilever with a 2 μm probe above the surface of the TM and acquired force-distance curves. In this study, all measurements were focused on the HC zone of the TM, along the length of the cochlea. The HC zone of the TM is likely the most relevant region for elucidating the mechanical role of the TM, because it is the zone in which OHC stereocilia are physically embedded into the TM. In addition, the most significant structural changes in the hetero- and homozygotes were observed in the HC zone. The Young's modulus values were estimated on the basis of a modified Hertz model as previously described (4).

The normal Young's modulus (E_z) of WT, hetero-, and homozygous TM samples as a function of cochlear longitudinal position is shown in Fig. 5. The E_z-values in the apical region of the WT and heterozygous are very similar: 27 ± 2 and 24 ± 4 kPa, respectively. The similarity in the E_z-values of the apical region is in agreement with our structural analysis, which reveals similar morphology and collagen architectures. The E_z-values are nearly twofold lower in homozygous TM than in WT and heterozygous TM. This decrease in E_z presumably reflects the lower fiber density we observed (Fig. 3).

In the middle and basal regions of the cochlea, differences in the mechanical properties of the TM are observed between all three genotypes. The Young's modulus values of mutated TM samples isolated from the mid-turn region of the cochlea are lower than those of their WT counterpart (49 ± 9 and 33 ± 5 kPa for the heterozygote and homozygote, respectively, compared with 109 ± 11 kPa for the WT). The most dramatic changes in E_z between mutated and WT TMs are observed in the basal part of the cochlea. The Young's moduli of hetero- and homozygous TM samples (75 ± 11 and 45 ± 7 kPa) are four and nearly seven times smaller than that of the WT TM (295 ± 15 kPa). In the WT TM, a gradual increase in the TM's E_z along the length of the cochlea is observed resulting in the

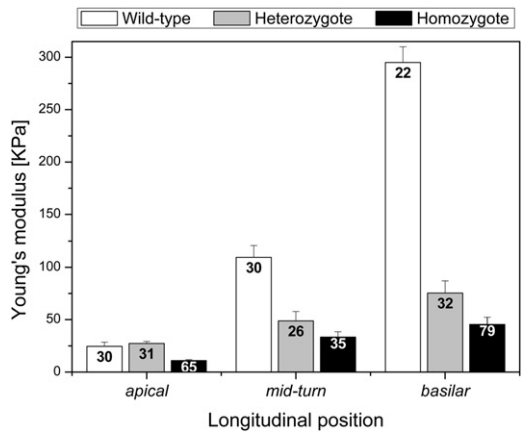

FIGURE 5 Longitudinal distribution of TM lateral Young's modulus values measured with a micrometer-scaled probe (radius = 1 μm). Measurements were localized to the radial zone that is situated above the HCs and is probably the most functionally relevant region of the TM. Results are grouped into three longitudinal regions: apical, mid-turn, and basal. WT, heterozygous, and homozygous samples are colored in white, gray, and black, respectively. The maximal loading force in all measurements was 25–30 nN. The bars represent the standard error, and the number of samples analyzed is indicated by the number shown in each column.

basal end being nearly 10 times stiffer than the apical end. This longitudinal gradient is significantly decreased in the heterozygous TM and even more so in the homozygous TM (Fig. 5). Overall, the apical E_z-values of both mutated TM variants are moderately changed throughout the entire length of the cochlea.

A 3D structural analysis of the TM reveals marked changes in the organization of the fibers in the basal region that correlate with the results obtained from the indentation assays. In the basilar region of the WT TM, the fibers are tightly arranged in a parallel orientation with respect to each other and to the plane of the TM's surface. In contrast, the morphology and structure in the basilar region of hetero- and homozygous TM samples resemble the structure of the apical region. The collagen fibers in the basilar region of mutated TM variants are oriented nearly perpendicularly to the surface direction of the sample (Fig. 3). Moreover, along the end of the WT TM, in the basilar HC zone, an intensified signal representing the merging of several fibers into thick fibers is observed (19). This marginal band forms a shell-like structure that engulfs the surface of the TM, and has been postulated to give rise to the increased stiffness of this region. In the hetero- and homozygous TM samples, the absence of this shell-like structure, as well as the apical-like collagen orientation, is likely to reduce the Young's modulus of the basilar region.

A central question in all studies that characterize the mechanical properties of the TM is, what role do these properties play in the mechanics of hearing? In the *Tecta* homozygous mice examined in this study, it is difficult to correlate the observed changes in mechanical properties with the physiological phenotype, since the TM was completely detached from the HC stereocilia. In the heterozygous mice, however, the TM was found to be in physical contact with one row of HC stereocilium bundles. Of interest, *Tecta* heterozygous mice were found to be mostly hearing-impaired at the higher frequencies, which raises the intriguing possibility that the observed hearing loss and the marked changes in the TM mechanical properties are connected. The lack of stereocilin immunolabeling in the first row of OHCs in the heterozygote mice confirms the loose nature of the HC area of the TM, which is normally highly organized and tightly packed. However, the lack of stereocilin immunolabeling should not be interpreted to mean that the stereocilia are not mechanically stimulated by the TM. Indeed, stereocilin-deficient mice show very little congenital hearing loss even though they have a lack of distortion product generation and progressive hearing loss (15). Similarly, our previous studies of calcium imaging of the first row of OHCs in heterozygote mice ex vivo and cochlear microphonic measurements in vivo demonstrated results consistent with normal forward transduction (13). Recently, we studied spatial variation in the material properties of WT TM using axial-indentation and lateral-force spectroscopy (8). By combining the experimental data with finite-element simulations, we found that the lateral Young's moduli of the TM are significantly lower than the axial modulus along its entire length. As a result, the TM has greater resistance to the vertical motion of stereocilia than to their lateral motion, which consequently deflects them. Using the values derived from this method, we then simulated the interactions between the TM and the embedded stereocilia. Of note, with these parameters, the stereocilia were deflected laterally when pushed into the TM, suggesting that stereocilia deflection is guided by TM anisotropy. In this study, we hypothesize that changes in the anisotropic mechanical properties of the heterozygous TM in the basal region prevented stereocilia deflection, thereby contributing to the high-frequency hearing loss.

To test this hypothesis, we measured the lateral properties of heterozygous TM samples. Before each lateral-force measurement, we applied a standard force-distance curve to estimate the normal Young's modulus of the sample. From the force-distance curve we also determined the TM indentation depth generated by a given loading force. All lateral-force measurements were performed at an indentation depth of 200 nm, which is similar to the depth at which OHC stereocilia are embedded in the TM. In similarity to a normal Young's modulus, the lateral force of heterozygous TM samples at their basal end (1.8 ± 0.9 nN, $n = 9$) is similar to that of apical WT (1.9 ± 0.2 nN (8)) and

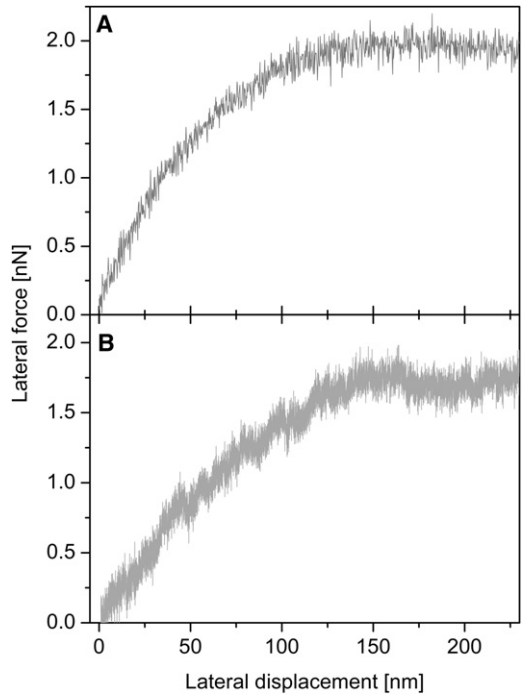

FIGURE 6 Typical averaged lateral-force curves for (*A*) WT and (*B*) heterozygous TM samples isolated from the apical region of the cochlea. No significant differences between the two curves are observed. Both curves arrive at a similar maximal lateral-force value of ~2 nN after lateral compression of 150–200 nm.

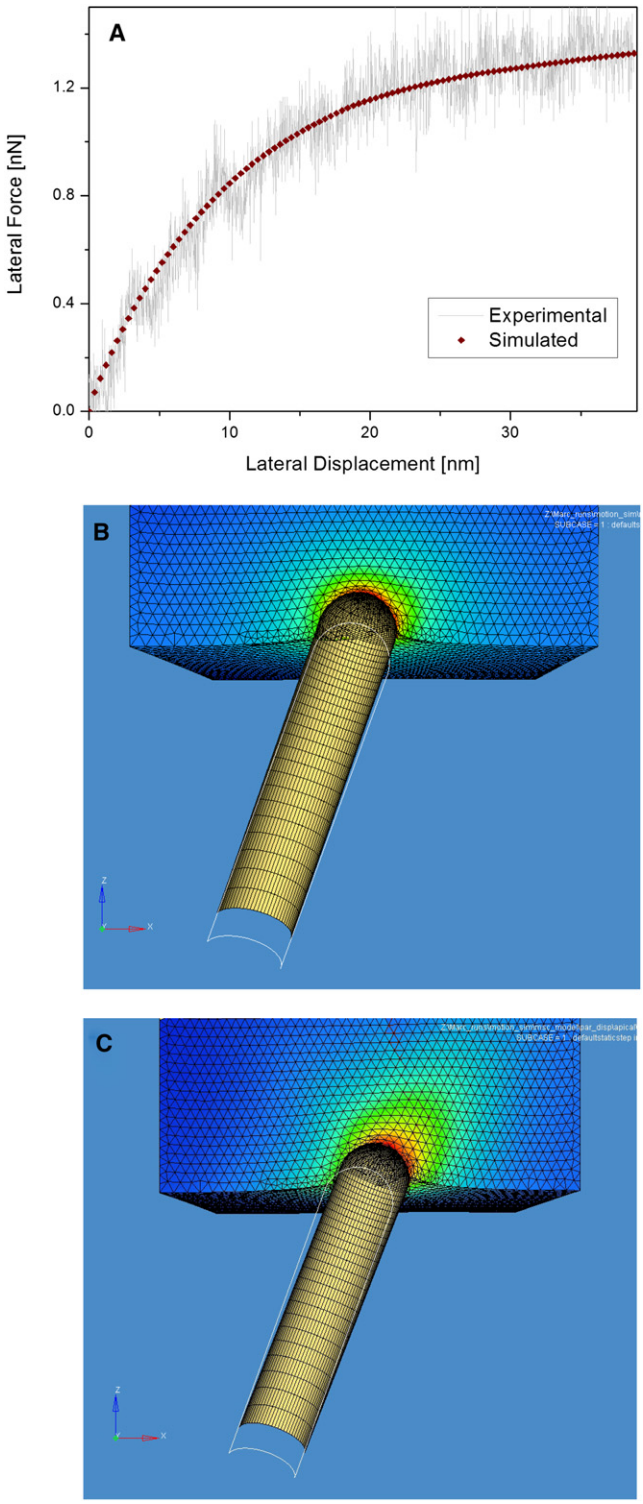

FIGURE 7 Estimating the lateral mechanical properties of a basilar heterozygous TM and the mechanical interactions between the basilar heterozygous TM and stereocilia by lateral-force spectroscopy and FE analysis. (*A*) Simulated (*dots*) versus an experimental (*solid gray line*) lateral-force curve for the TM. The curve reaches a maximal lateral-force value of ~1.2 nN after lateral compression of 25–30 nm. A normal Young's modulus of 40 KPa was obtained from an indentation-type experiment. The best fit was obtained by optimizing the lateral mechanical properties of the model TM. (*B*) Deflection of the stereocilium as it is pushed against a basilar heterozygous TM model. The TM is modeled as an elastic 3D plate made of anisotropic material with $E_x = 180$, $E_y = 140$, and $E_z = 40$ kPa. The stereocilium is modeled as a nondeformable rod (150 nm in diameter) capped by a sphere at its tip, implanted 100 nm into the TM. The base of the stereocilium is moved vertically along its longitudinal axes. (*C*) Deflection of the stereocilium as it is pushed against an apical heterozygous TM model.

heterozygous (1.8 ± 0.8, $n = 6$) TM samples. Analysis of the shape of the lateral-force curve reveals an important difference between the basilar region of the heterozygous mutant and the apical regions of the WT or heterozygous mutant. In the apical regions of heterozygous and WT samples, a relatively large lateral compression (~200 nm) is required to generate maximal lateral force (Fig. 6), whereas a much smaller compression (25–30 nm) is required in the basilar region of the heterozygous TM to generate a similar maximal lateral force (Fig. 7 *A*). Assuming a simple spring model, where stiffness is defined as the ratio between force and displacement, the above lateral-force results imply that the lateral stiffness of a heterozygous TM at its basal end is significantly higher than at its apical end and in the apical region of a WT TM.

To evaluate the relationships between the mechanical properties of the basilar heterozygous TM along the different axes, we compared the corresponding Young's moduli: E_x, E_y (parallel and perpendicular to the radial direction, respectively) and E_z. To obtain the lateral moduli (E_x and E_y), we used a methodology developed in our laboratory (8). We first simulated the lateral-force measurements using the finite-element (FE) method, and modeled the TM as an anisotropic material characterized by three independent Young's moduli (E_x, E_y, and E_z). Whereas E_x and E_y are free parameters, E_z is a constant that is determined experimentally from the normal force-distance curve. The model properties that best fit our force measurements were considered as the estimated TM lateral moduli (Fig. 7 *A*). The FE analysis results for the basilar heterozygous TM indicate that, in contrast to its apical region and to the basilar region of the WT TM, both of the lateral moduli (E_x and $E_y = 180$ and 140 kPa, respectively) are significantly higher than the normal modulus ($E_z = 40$ kPa).

Finally, we simulated the mechanical interactions between the basilar heterozygous TM and the embedded stereocilia using the FE method as previously described (8). The TM was modeled as an elastic 3D plate. To simulate in vivo motion, the stereocilium was pushed against the TM along its longitudinal axis (Fig. 7 *B*), and rotational movements were unconstrained. Of note, when the TM is modeled as an anisotropic material with mechanical properties taken from the basilar heterozygous analysis, the stereocilium maintains its initial orientation and the vertical motion of the base is not converted into a lateral deflection

of its tip (Fig. 7 *B*). By contrast, when the apical heterozygous TM is modeled, the vertical motion of the base of the stereocilium is converted into a lateral deflection of its tip (Fig. 7 *C*).

In conclusion, this study highlights the interrelations among the structure, material properties, and function of the TM. Our analysis of the mechanical and structural changes induced by *Tecta* mutations strengthens the linkage between them. The most prominent changes were localized to the cochlear partition that was previously shown to be the most affected physiologically (13). Although these findings demonstrate a correlation between the material properties of the TM and its physiological function, they do not provide a mechanism. Recently, we proposed that stereocilia deflection is guided by the anisotropic properties of the TM (8). In this study, we find that the anisotropic properties of heterozygous *Tecta* TMs differ from those of the WT predominantly in the high-frequency region of the cochlea. This finding provides a mechanical explanation for the hearing loss observed in humans who carry the *Tecta* mutation (14).

Although other forces, such as fluid motion, may play a role in stereocilia deflection, our results strongly support the hypothesis that the material properties of the TM play a crucial role in this process, which is a key factor in hearing. One caveat, however, is that our mechanical data were not collected at acoustical frequencies. The ultimate impact on stereociliary deflection and bundle stress is also likely to be influenced by the frequency characteristics of the TM's mechanical properties. Further studies and modeling will help to elucidate the nature of these effects. Nevertheless, we can conclude from the data presented here that large, region-dependent alterations in TM mechanics can be generated by single-point mutations in α-tectorin. Thus, the integration of α-tectorin into the TM has regional gradients, and changes in this process produce tonotopic gradients in HC stimulation.

SUPPORTING MATERIAL

A figure is available at http://www.biophysj.org/biophysj/supplemental/S0006-3495(11)00469-3.

We thank Yehudit Hermesh for technical assistance in the surgical procedure performed on the animals, Yaron Silberberg for providing access to his SHIM and THIM setups, David Barlam for assistance in the FE modeling, and Christine Petit for providing the stereocilin antibody.

This work was supported in part by the Israel Science Foundation (grant 26/05), the Minerva Foundation with funding from the Federal German Ministry of Education and Research, and the National Institute on Deafness and Other Communication Disorders, National Institutes of Health (K08 DC006671 and P30 DC010363 to J.S.O.). I.R. holds the Robert Edwards and Roselyn Rich Manson Career Development Chair. The EM studies were conducted at the Irving and Cherna Moskowitz Center for Nano and Bio-Nano Imaging at the Weizmann Institute of Science.

REFERENCES

1. Goodyear, R. J., and G. P. Richardson. 2002. Extracellular matrices associated with the apical surfaces of sensory epithelia in the inner ear: molecular and structural diversity. *J. Neurobiol.* 53:212–227.
2. Hasko, J. A., and G. P. Richardson. 1988. The ultrastructural organization and properties of the mouse tectorial membrane matrix. *Hear. Res.* 35:21–38.
3. Tsuprun, V., and P. Santi. 1997. Ultrastructural organization of proteoglycans and fibrillar matrix of the tectorial membrane. *Hear. Res.* 110:107–118.
4. Gueta, R., D. Barlam, …, I. Rousso. 2006. Measurement of the mechanical properties of isolated tectorial membrane using atomic force microscopy. *Proc. Natl. Acad. Sci. USA.* 103:14790–14795.
5. Abnet, C. C., and D. M. Freeman. 2000. Deformations of the isolated mouse tectorial membrane produced by oscillatory forces. *Hear. Res.* 144:29–46.
6. Freeman, D. M., C. C. Abnet, …, T. F. Weiss. 2003. Dynamic material properties of the tectorial membrane: a summary. *Hear. Res.* 180:1–10.
7. Gavara, N., and R. S. Chadwick. 2009. Collagen-based mechanical anisotropy of the tectorial membrane: implications for inter-row coupling of outer hair cell bundles. *PLoS ONE.* 4:e4877.
8. Gueta, R., D. Barlam, …, I. Rousso. 2008. Sound-evoked deflections of outer hair cell stereocilia arise from tectorial membrane anisotropy. *Biophys. J.* 94:4570–4576.
9. McGuirt, W. T., S. D. Prasad, …, R. J. Smith. 1999. Mutations in COL11A2 cause non-syndromic hearing loss (DFNA13). *Nat. Genet.* 23:413–419.
10. Masaki, K., J. W. Gu, …, A. J. Aranyosi. 2009. Col11a2 deletion reveals the molecular basis for tectorial membrane mechanical anisotropy. *Biophys. J.* 96:4717–4724.
11. Ghaffari, R., A. J. Aranyosi, and D. M. Freeman. 2007. Longitudinally propagating traveling waves of the mammalian tectorial membrane. *Proc. Natl. Acad. Sci. USA.* 104:16510–16515.
12. Richter, C. P., G. Emadi, …, P. Dallos. 2007. Tectorial membrane stiffness gradients. *Biophys. J.* 93:2265–2276.
13. Xia, A., S. S. Gao, …, J. S. Oghalai. 2010. Deficient forward transduction and enhanced reverse transduction in the α tectorin C1509G human hearing loss mutation. *Dis. Model Mech.* 3:209–223.
14. Pfister, M., H. Thiele, …, S. Kupka. 2004. A genotype-phenotype correlation with gender-effect for hearing impairment caused by *Tecta* mutations. *Cell. Physiol. Biochem.* 14:369–376.
15. Verpy, E., M. Leibovici, …, C. Petit. 2011. Stereocilin connects outer hair cell stereocilia to one another and to the tectorial membrane. *J. Comp. Neurol.* 519:194–210.
16. Hutter, J., and J. Bechhoeffer. 1993. Calibration of atomic-force microscope tips. *Rev. Sci. Instrum.* 64:1868–1873.
17. Ruan, J. A., and B. Bhushan. 1994. Atomic-scale friction measurements using friction force microscopy 0.1. General principles and new measurement techniques. *ASME J. Tribol.* 116:378–388.
18. Mohler, W., A. C. Millard, and P. J. Campagnola. 2003. Second harmonic generation imaging of endogenous structural proteins. *Methods.* 29:97–109.
19. Gueta, R., E. Tal, …, I. Rousso. 2007. The 3D structure of the tectorial membrane determined by second-harmonic imaging microscopy. *J. Struct. Biol.* 159:103–110.
20. Yelin, D., and Y. Silberberg. 1999. Laser scanning third-harmonic-generation microscopy in biology. *Opt. Express.* 5:169–175.
21. Verpy, E., S. Masmoudi, …, C. Petit. 2001. Mutations in a new gene encoding a protein of the hair bundle cause non-syndromic deafness at the DFNB16 locus. *Nat. Genet.* 29:345–349.
22. Jovine, L., J. Park, and P. M. Wassarman. 2002. Sequence similarity between stereocilin and otoancorin points to a unified mechanism for mechanotransduction in the mammalian inner ear. *BMC Cell Biol.* 3:28.